ChemBioChem

Research Article
doi.org/10.1002/cbic.202500195

Chemistry Europe
European Chemical Societies Publishing

www.chembiochem.org

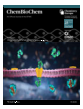

Chromenone Derivatives as CRM1 Inhibitors for Targeting Glioblastoma

Salvatore Princiotto, Lucía Jiménez, Lucía Domínguez, João G. N. Sequeira, Cristiana Mourato, Alba Orea-Soufi, Bruno Santos, Sabrina Dallavalle, Miguel Machuqueiro, Bibiana I. Ferreira,* and Wolfgang Link*

Glioblastoma (GBM) is one of the most aggressive and deadly cancers. Due to the complexity and redundancy within signaling networks in GBM, targeted inhibitors of specific pathways have shown only limited success. The nuclear export receptor chromosome region maintenance 1 (CRM1) has recently emerged as a promising therapeutic target, as its inhibition can simultaneously disrupt multiple key oncogenic drivers. Herein, whether chromenone derivatives, known for detecting thiol-containing molecules, can function as CRM1 inhibitors is explored. Several chromenone-based derivatives are synthesized and it is demonstrated that they inhibit CRM1-driven nuclear export in a structure- and dose-dependent manner. A preliminary structure–activity relationship is established, providing a rationale for selective CRM1 binding based on molecular docking studies. Additionally, it is showed that the active chromenone derivatives effectively inhibit the nuclear export of endogenous nuclear export signal-containing substrates in GBM cells. Several of these compounds exhibit selective cytotoxicity against GBM cell lines, highlighting their potential as targeted therapies for GBM.

1. Introduction

Glioblastoma (GBM) is the most prevalent and lethal brain tumor in adults.[1] Current treatment follows the "Stupp protocol" which combines surgical resection (when feasible), radiotherapy, and concomitant temozolomide (TMZ) chemotherapy.[2] However, even with this aggressive treatment regimen, GBMs remain incurable and nearly always recur.

1.1. Glioblastomas (GBMs) Evade Therapy through Redundancy in Key Signaling Pathways

Three key signaling pathways are consistently disrupted in GBM: the receptor tyrosine kinase (RTK)/PI3K/AKT/FOXO pathway, as well as the p53 and Rb1 tumor suppressor pathways.[3,4] Despite the development of inhibitors targeting RTKs, PI3K, or mTOR, their therapeutic effects in GBM have been modest.[5] This is largely due to substantial redundancy within these pathways, which enables GBM cells to adapt and evade targeted therapies, ultimately leading to treatment failure. Therefore, simultaneously targeting multiple oncogenic pathways may offer a more effective therapeutic strategy.

1.2. Nuclear Export Inhibition Targets Multiple Oncogenic Pathways in Glioblastoma (GBM)

One promising emerging approach is nuclear export inhibition. Several key proteins in GBM rely on their intracellular localization for activity, and the best-studied nuclear export receptor, chromosome region maintenance 1 (CRM1, also known as XPO1 or exportin 1),[6] plays a pivotal role in the progression of various cancers, including GBM.[7–9] Proteins destined for export through the nuclear pore complex typically possess a nuclear export signal (NES) that binds to CRM1.[10] CRM1 is the primary nuclear export receptor for numerous tumor suppressors and oncogenic proteins,[11] including Rb1, FOXO proteins, p53, p21, p27, survivin, and eIF4E, all of which play crucial roles in GBM and are

S. Princiotto, S. Dallavalle
DeFENS Department of Food, Environmental and Nutritional Sciences
Università degli Studi di Milano
Via Festa del Perdono, 720122 Milan, Italy

L. Jiménez, L. Domínguez, W. Link
Sols-Morreale Biomedical Research Institute (IIBM)
Spanish National Research Council (CSIC)
Universidad Autónoma de Madrid (UAM)
Calle Arturo Duperier, 428029 Madrid, Spain
E-mail: walink@iib.uam.es

C. Mourato, A. Orea-Soufi, B. Santos, B. I. Ferreira
Algarve Biomedical Center Research Institute-ABC-RI
University of Algarve
Campus of Gambelas, 8005-139 Faro, Portugal
E-mail: biferreira@ualg.pt

C. Mourato, A. Orea-Soufi, B. Santos, B. I. Ferreira
Faculty of Medicine and Biomedical Sciences
University of Algarve
Campus de Gambelas, 8005-139 Faro, Portugal

J. G. N. Sequeira, M. Machuqueiro
BioISI–Instituto de Biossistemas e Ciências Integrativas
Faculdade de Ciências
Universidade de Lisboa
Campo Grande, 1749-016 Lisbon, Portugal

Supporting information for this article is available on the WWW under https://doi.org/10.1002/cbic.202500195

frequently mislocalized in cancer cells. Notably, CRM1 expression is elevated in GBM,[8,9] with its level of expression directly correlating with glioma tumor grade and inversely with patient survival.[7,12] Moreover, CRM1 has been implicated in resistance to TMZ treatment.[8,13] Supporting this, studies have shown that nuclear-trapped tumor suppressors like survivin can sensitize GBM cells to TMZ.[13] These findings collectively establish CRM1 as a highly promising target for the development of novel GBM therapies.

1.3. Chromosomal Region Maintenance 1 Inhibitors have Reached the Clinic

Accordingly, several generations of CRM1 inhibitors have been developed,[14] with selinexor emerging as the first CRM1 inhibitor approved for the treatment of patients with multiple myeloma and diffuse large B-cell lymphoma.[15] In addition, selinexor is currently being evaluated in clinical trials for its potential use in treating GBM. CRM1 inhibitors typically contain an electrophilic group that specifically react with nucleophilic residues like cysteine in proteins. The presence of the thiol (—SH) group makes the cysteine at position 528 of human CRM1 a suitable nucleophile ready to attack electrophilic centers, especially under physiological conditions. The resulting covalent bond between the inhibitor and the cysteine residue prevents CRM1 from interacting with its substrates.

1.4. Chromenone Compounds can Detect Thiol-Containing Proteins

Due to their electrophilic α,β-unsaturated system, chromenones (**Figure 1**) have been shown to function as a probe for detecting thiol-containing molecules.[16–19] These evidences prompted us to investigate the potential effect of chromenone-containing compounds on CRM1 activity.

2. Results

2.1. A Chromenone Derivative Inhibits Chromosomal Region Maintenance 1-Dependent Nuclear Export

A representative in-house chromenone derivative **1** was tested for its ability to inhibit human CRM1 activity. To do so, we employed a high-content screening (HCS) system using a coculture of two established reporter osteosarcoma cell lines (U2OS). The first, U2redNES, expresses the viral protein REV fused to a NES and a red fluorescent protein (RFP). The second, U2foxRELOC, stably expresses the FOXO3 transcription factor fused to GFP, also containing a NES.[20]

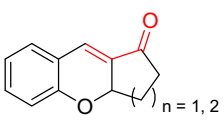

Figure 1. General structure of the chromenone moiety (α,β-unsaturated system in red).

Following an incubation of 1 h, fluorescence microscopy was used to assess the subcellular localization of the reporter proteins. 1% aqueous dimethyl sulfoxide (DMSO) was used as negative control.[21] In DMSO-treated cells, both fluorescent reporter proteins displayed predominantly cytoplasmic localization. Treatment with 25 μM LY294002, a known pan-PI3K inhibitor,[22] caused nuclear translocation of FOXO-GFP without altering the subcellular localization of the red fluorescent reporter protein (**Figure 2**B). As expected, 100 nM selinexor, a CRM1 inhibitor, retained both the red and green fluorescent proteins within the nucleus, confirming CRM1 inhibition (Figure 2C). Similarly, treatment with 1 at concentrations of 10, 25, and 50 μM induced nuclear retention of both reporter proteins, indicating that the chromenone derivative interfered with CRM1-mediated nuclear export (Figure 2D–F). These results show that 1 effectively inhibits the export activity of human CRM1.

2.2. Analogues of Compound 1 also Inhibit Chromosomal Region Maintenance 1(CRM1)

The above-reported data showed that chromenone compound **1** could inhibit CRM1. Indeed, it has already been reported that such moieties could be exploited as colorimetric probes for the detection of thiol-containing amino acids and peptides.[23,24] Based on this, we synthesized and tested a small collection of analogs of compound **1**, variously substituted at position 7 and featured by a fused five- or six-membered carbonyl-containing ring (**Figure 3**). Chromenones **1**-**8** were synthesized by the reaction of a suitable salicylaldehyde and 2-cyclopenten-1-one or 2-cyclohexen-1-one via Baylis-Hillman and intramolecular Michael addition in the presence of imidazole,[23] as reported in Figure 3B.

The inhibitory potential of these compounds was assessed at two concentrations using the multiplexed HCS system. Among the eight chromenone analogs tested, three compounds—**6**, **2**, and **8**—demonstrated no activity at either concentration (data not shown). In contrast, five compounds showed activity. Four of these—**5**, **1**, **3**, and **4**—were active at both concentrations tested. However, compound 7 displayed activity at 10 μM, but exhibited slight toxicity at that concentration and became lethal to the cells at higher concentrations. Therefore, compound **7** was excluded from most of the subsequent experiments. Based on the analysis of both the active and inactive structures, we hypothesize that analogs containing the cyclopentanone derivative have some advantage over the ones with cyclohexanone. This effect can be manifested through some binding advantage to CRM1-binding pocket (the NES-binding groove) or just by making its double bond located in C3 and C4 become more susceptible to the Cysteine 528 (Cys528) thiolate attack.

2.3. A Preliminary Structure–Activity Relationship Analysis Provides Structural Insights

To establish a preliminary structure–activity relationship (SAR), we further evaluated the dose-dependent inhibitory effects of the active compounds across ten different concentrations using the HCS system. **Table 1** and Figure S1 (Supporting Information)

Research Article
doi.org/10.1002/cbic.202500195
Chemistry Europe
European Chemical Societies Publishing

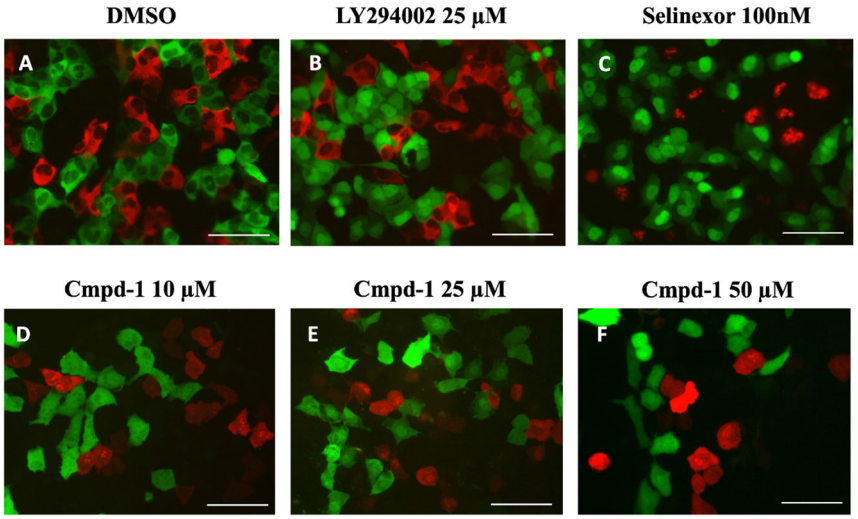

Figure 2. Subcellular localization of green and red reporter proteins in U2OS exposed to 1. U2foxRELOX and U2redNES cells were coculture in 96-well plates and treated for 1 h with A) 1% DMSO, B) 25 μM LY294002, C) 100 nM Selinexor, D) 10 μM compound **1**, E) 25 μM compound **1**, and F) 50 μM compound **1**. After compound treatment, cells were fixed, and images were acquired using fluorescent microscopy. Scale bar: 100 μm.

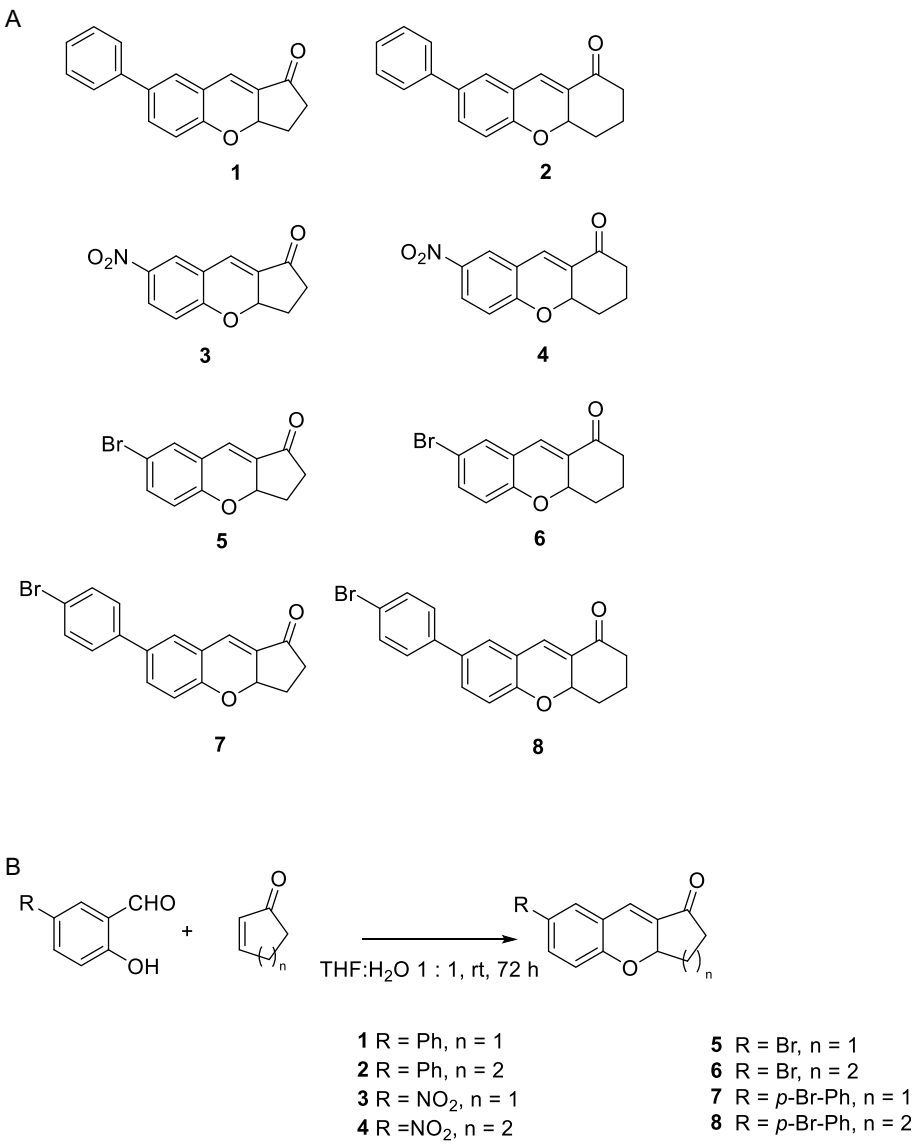

Figure 3. A) Chromenones **1**, **3**, and structural analogs **4**-**8**. B) Synthesis of compounds **1**-**8** from 2-hydroxybenzaldehydes and cyclic enones.

Table 1. EC50 for each reporter protein and compound treatment. Nuclear retention extrapolated from the dose–response graphs (Figure S1, Supporting Information). Mean EC50 ± standard deviation values for each hit compound are depicted ($N = 3$).

Compound	EC50 [μM] U2foxRELOC	EC50 [μM] U2redNES	Mean EC50 [μM]
1	19.6 ± 2.9	17.3 ± 1.8	18.5 ± 1.6
5	4.4 ± 0.3	4.4 ± 0.1	4.4 ± 0
3	35.5 ± 0.9	37.8 ± 0.3	36.7 ± 2.9
4	102.3 ± 0.7	103.0 ± 2.2	102.7 ± 0.5

present the EC50 values of the four active compounds, along with the parent compound **1**, for each reporter cell line. Importantly, EC50 values for the FOXO and NES reporter cells are quite similar, indicating that FOXO3 nuclear export is strictly NES-dependent.

The activity of compound **4** on the tested cell lines was significantly lower than its five-membered analog **3**. This result indicates that the ring strain could affect the reactivity toward the cysteine-containing CRM1. Seven-bromo-substituted compound **5** resulted as the best of the series, inducing a fourfold inhibition compared to parent compound 1, and a ninefold inhibition against the nitro derivative (compound **3**). Based on the mechanism suggested by Huo et al.,[23] we investigated the relationship between the structure of the selected compounds and the effect on U2foxRELOX and U2redNES cells.

2.4. Molecular Docking Calculations to Identify the Most Promising Binding Modes to Chromosomal Region Maintenance 1 (CRM1)

To rationalize the reactivity of the tested compounds, we modeled their binding modes to the NES binding groove of CRM1 and estimated their susceptibility to bind covalently to this protein. We employed an ensemble docking protocol, where the CRM1 conformational space was explored by extensive molecular dynamics (MD) simulations. The docking solutions at the end of the pipeline were analyzed in terms of how susceptible their double bond (in particular C4) is to be attacked nucleophilically by the Cys528 thiolate[23] (see Ensemble Docking section in Materials and Methods). We selected the most promising binding poses of each compound following a geometric criterium and reported their docking binding energies (**Table 2** and Figure S2, Supporting Information).

All compounds can bind to the Φ3 site of the NES-binding groove, in a conformation that allows a Cys528 nucleophilic attack, while some also occupy the Φ4 or Φ2 sites (**Figure 4** and Figure S2, Supporting Information). Since the binding energies obtained (Table 1) do not correlate well with the compound's ability to modulate CRM1 activity, it suggests that the noncovalent binding is not the rate-limiting step of CRM1 inhibition. Indeed, the electrophilic nature of the analog double bond may play a crucial role in this process. The in vitro activity assays identified all chromenone compounds with a five-membered carbonyl-containing ring (marked with an asterisk in Table 2) to be able to modulate CRM1 activity, with **7** becoming too toxic at slightly higher concentrations. The only chromenone compound with a six-membered carbonyl-containing ring with CRM1 activity modulation capacity was

Table 2. Molecular docking binding energy values (kcal mol^{-1}) obtained for the best-aligned binding modes of each of the studied compounds.

Compound	Binding energy [kcal mol^{-1}]
1*	−7.7
3*	−6.7
5*	−6.8
7*	−8.0
2	−7.3
4	−7.6
6	−6.8
8	−8.6

Compounds with a five-membered carbonyl-containing ring are highlighted with an asterisk. Since these binding modes have the chromenone analogs optimally located to be covalently attacked by Cys528, their energy values may not correspond to the lowest ones obtained in the docking protocol.

compound **4** that, as compound **3**, has a nitro group that is predicted to interact with at least one of two Lysines (Lys 537 and Lys 568) in the NES-binding groove (Figure 4). The nitro group also has an electron-withdrawing effect on C4, enhancing its electrophilic nature. This electronic effect and the potentially better alignment for the Cys528 nucleophilic attack may be offsetting the negative effect of having the six-membered carbonyl-containing ring.

To further explore these two factors, the electronic effects on the analogs' double bond and the structural alignment for Cys528 nucleophilic attack, we compared the binding modes of compound **1** (inhibitor) and **2** (noninhibitor) (Figure 4C). Their nearly identical binding poses and very similar binding energies (Table 2) indicate that the observed activity difference needs to be primarily correlated with the electrophilicity of the double bond that seems to be higher in the five-membered ring analogs, compared with the six ones. These results show that when designing CRM1 covalent inhibitors, attention must be paid to the reactivity of the susceptible group since Cys528 reactivity strongly depends on this factor.

2.5. Active Chromenone Compounds also Affect Subcellular Localization of Endogenous Proteins

To ensure that the inhibitory effect of the hit compounds is not restricted to exogenous CRM1 substrates fused to fluorescent proteins, we examined their impact on the nuclear export of endogenous CRM1 substrates, including Ran-binding protein 1 (RANBP1) and E3 ubiquitin-protein ligase constitutive photomorphogenic 1 (COP1).[20] To this end, U2OS cells were treated with the active compounds for 1 h at concentrations determined by their respective EC50 values. Following treatment, the cells were fixed, permeabilized, and their nuclei stained with 4′,6-diamidino-2-phenylindole (DAPI). Subcellular localization of RANBP1 and COP1 was then analyzed. As shown in Figure S4 (Supporting Information), in the DMSO control, RANBP1 was predominantly localized in the cytoplasm. However, upon treatment with the compounds, RANBP1 accumulated in the nucleus, indicating that CRM1 inhibition affects the subcellular localization of endogenous CRM1 substrates. Similar results were observed for COP1 (Figure S4, Supporting Information).

Research Article
doi.org/10.1002/cbic.202500195
Chemistry Europe
European Chemical Societies Publishing

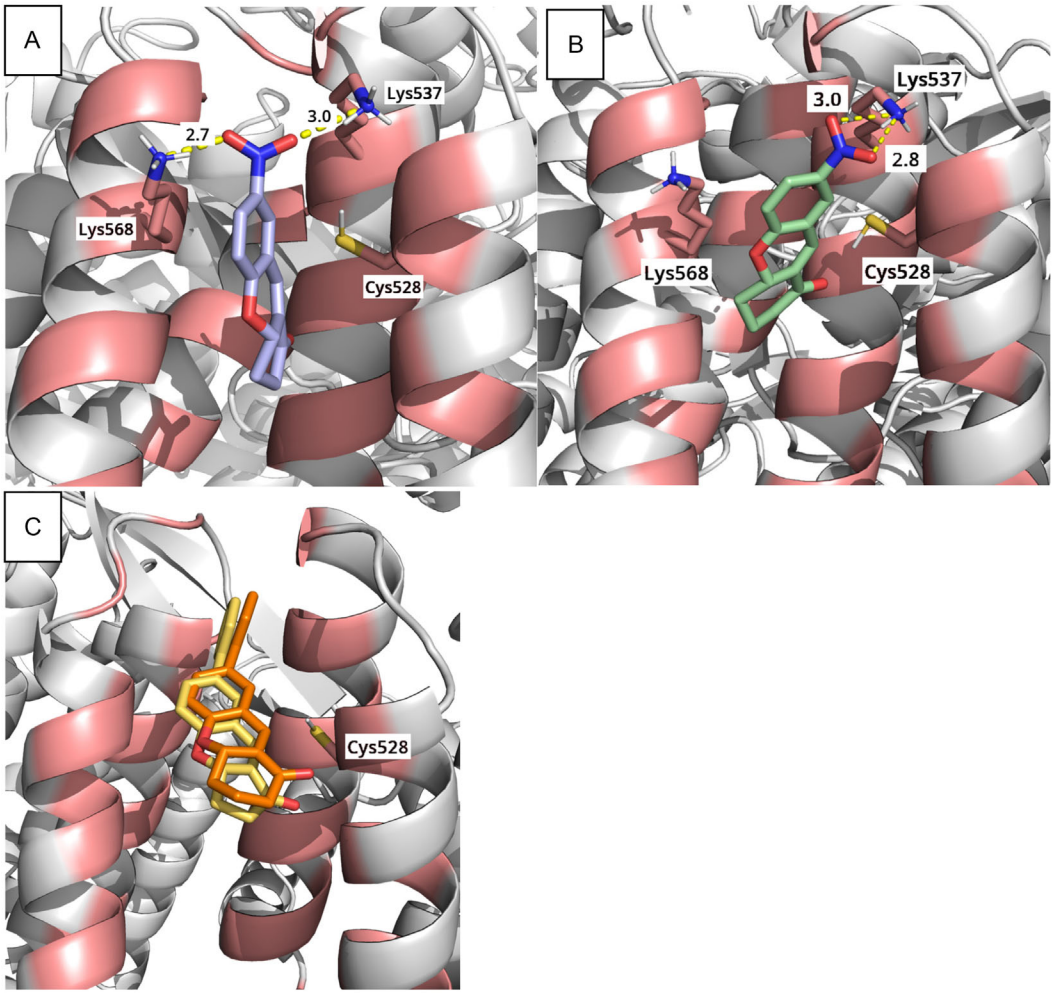

Figure 4. Binding modes of compound A) **1** and B) 4, which are represented as blue and green sticks, respectively. The strong interactions between the nitro group and the side chains of Lys537 and Lys568 are also represented (distances in Å). The CRM1 is shown in a gray cartoon with the residues involved in the NES-binding groove colored pink. The reactive Cys528 is also shown in sticks. C) Binding mode of a CRM1 activity modulator (compound **1**, yellow) and a very similar analog without CRM1 modulating capacity (compound **2**, orange). The CRM1 is shown in a gray cartoon with the residues involved in the NES-binding groove colored pink. The reactive Cys528 is also shown in sticks.

2.6. Nuclear Retention began at 30 min, and Cytotoxicity was Observed before 24 h of Incubation

To investigate the kinetics of CRM1 inhibition by the active analogs, we conducted time-course assays. Using the Cell Observer microscope, we monitored reporter cell lines for 24 h in the presence of the compounds at concentrations based on their EC50 values. DMSO had no effect on the cellular localization of the reporter proteins, which remained predominantly cytoplasmic throughout the experiment. In contrast, selinexor inhibited nuclear export, leading to the accumulation of both NES-RFP and FOXO-GFP in the nuclei. No signs of toxicity were observed with selinexor until after 30 h of treatment. The four active compounds increased nuclear retention within 20–30 min of exposure. While the inhibitory effect persisted, cell death occurred within 24 h upon the treatment with compounds **5**, **1**, and **4** (**Figure 5**). Additionally, U2foxRELOC cells were more sensitive to the treatments compared to U2redNES cells. Notably, cells treated with compound **3** remained attached and preserved their morphology, indicating that this compound does not exert acute cytotoxic effects (Figure 5J–L).

2.7. Compound Treatment also Inhibits Nuclear Export in Glioblastoma (GBM) Cell Lines

To evaluate the potential of the active chromenone analogs for treating GBM, their activity was tested in various GBM cell lines. Immunofluorescence assays were performed using LN229, SF268, U87, U118, and U251 cells, which were incubated with each compound for 1 h. Since GBM cell lines exhibited increased sensitivity to the hit compounds, the concentration used was reduced accordingly. Following treatments, we examined the localization of the FOXO3 protein using a specific antibody.[25] Unlike in U2OS WT cells, where nuclear retention of FOXO3 was more pronounced, in GBM cell lines, endogenous FOXO3 was initially distributed equally between the nucleus and cytoplasm under basal conditions with DMSO (Figure 6A–C). Despite this, all hit compounds induced a noticeable shift of FOXO3 fluorescence to

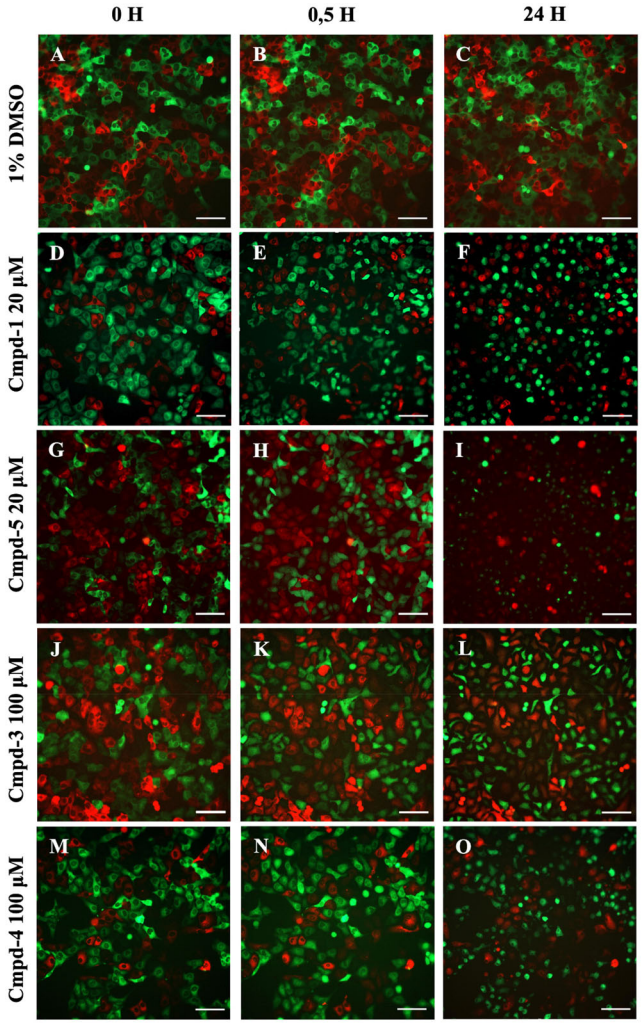

Figure 5. Subcellular localization and toxicity in reporter cells. Time-course experiment in cocultured U2foxRELOC and U2redNES cell lines during 24 h exposed to A–C) 1% DMSO, D–F) 20 μM compound **1**, G–I) 20 μM **5**, J–L) 100 μM **3**, and M–O) 100 μM **4**. Pictures shown represent the results at basal state, after 0.5 and 24 h of treatment. Scale bar: 100 μm.

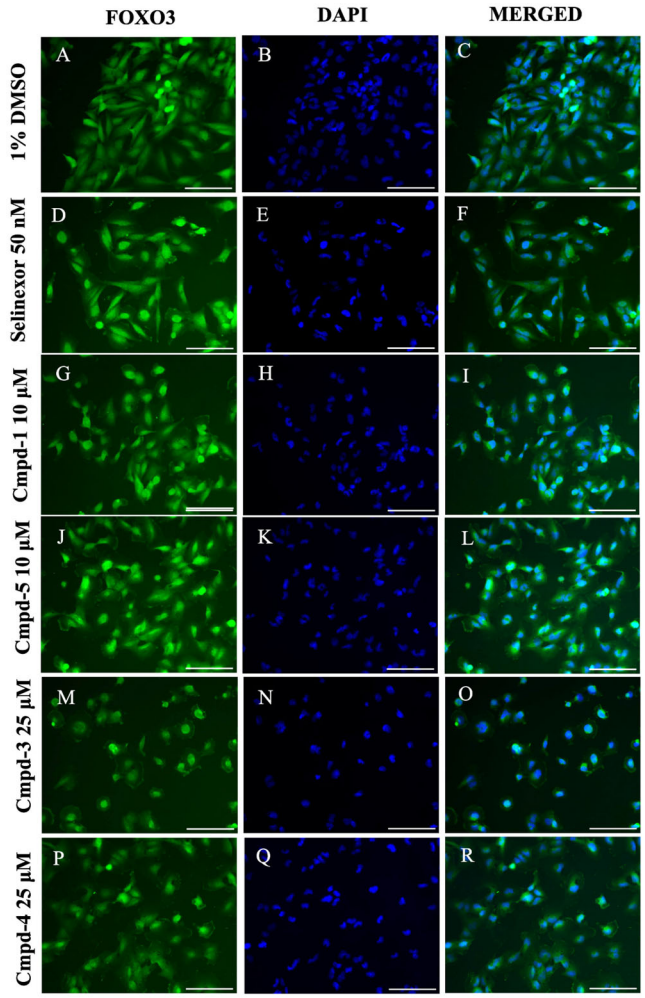

Figure 6. Subcellular localization of the endogenous FOXO3 protein in GB cells. U251 cells were treated for 1 h with A–C) 1% DMSO, D–F) 50 nM Selinexor, G–I) 10 μM compound **1**, J–L) 10 μM **5**, M–O) 25 μM **3**, and P–R) 25 μM **4**. Fixed cells were incubated with antibody against FOXO3, and then secondary green fluorescent antibody and nuclei were stained with DAPI. Images show the green (FOXO3), blue (DAPI), and merged channels, obtained with fluorescence microscopy. Scale bar: 100 μm.

the nucleus across all five GBM cell lines, resulting in a reduced cytoplasmic fluorescent signal. Representative results from the U251 cell line are shown in **Figure 6**. These data demonstrate that the chromenone analogs are capable of inhibiting nuclear export in GBM cells, supporting their potential use in GBM treatment.

2.8. Chromenone Analogs Exhibit Selective Cytotoxicity against GBM Cells

To assess the therapeutic potential of chromenone analogs against GBM cells, we compared the cytotoxicity of the active compounds in multiple GBM cell lines to that in the nontumoral CC2509 fibroblast cell line after 24, 48, and 72 h of incubation. Selinexor and TMZ, the standard chemotherapeutic for GBM, were used as controls. Cell viability was assessed using MTT assays, which measure the formation of formazan crystals and their absorbance at 570 nm. As shown in **Figure 7**, compounds **3** and **4** induced the highest levels of cytotoxicity across all cell lines at 24, 48, and 72 h. However, SF268 cells exhibited the highest resistance to these compounds, with 30% of cells surviving the treatment with compound **4** after 72 h, while other cell lines showed only 10% survival during the same period. Interestingly, although **5** did not demonstrate significant cytotoxicity at 24 or 48 h, it reduced cell viability to 10% after 72 h in nearly all GBM cell lines, except for SF268, where viability remained at 50%. Additionally, compound **1** only showed substantial cytotoxicity after 72 h, with GBM cell viability ranging from 10% to 50%.

This data reveals differential sensitivity between GBM and nontumoral fibroblast cells and the therapeutic potential of chromenone analogs as CRM1 inhibitors.

3. Discussion and Conclusions

CRM1 has emerged as a highly promising therapeutic target for GBM, as its inhibition disrupts multiple key driver pathways

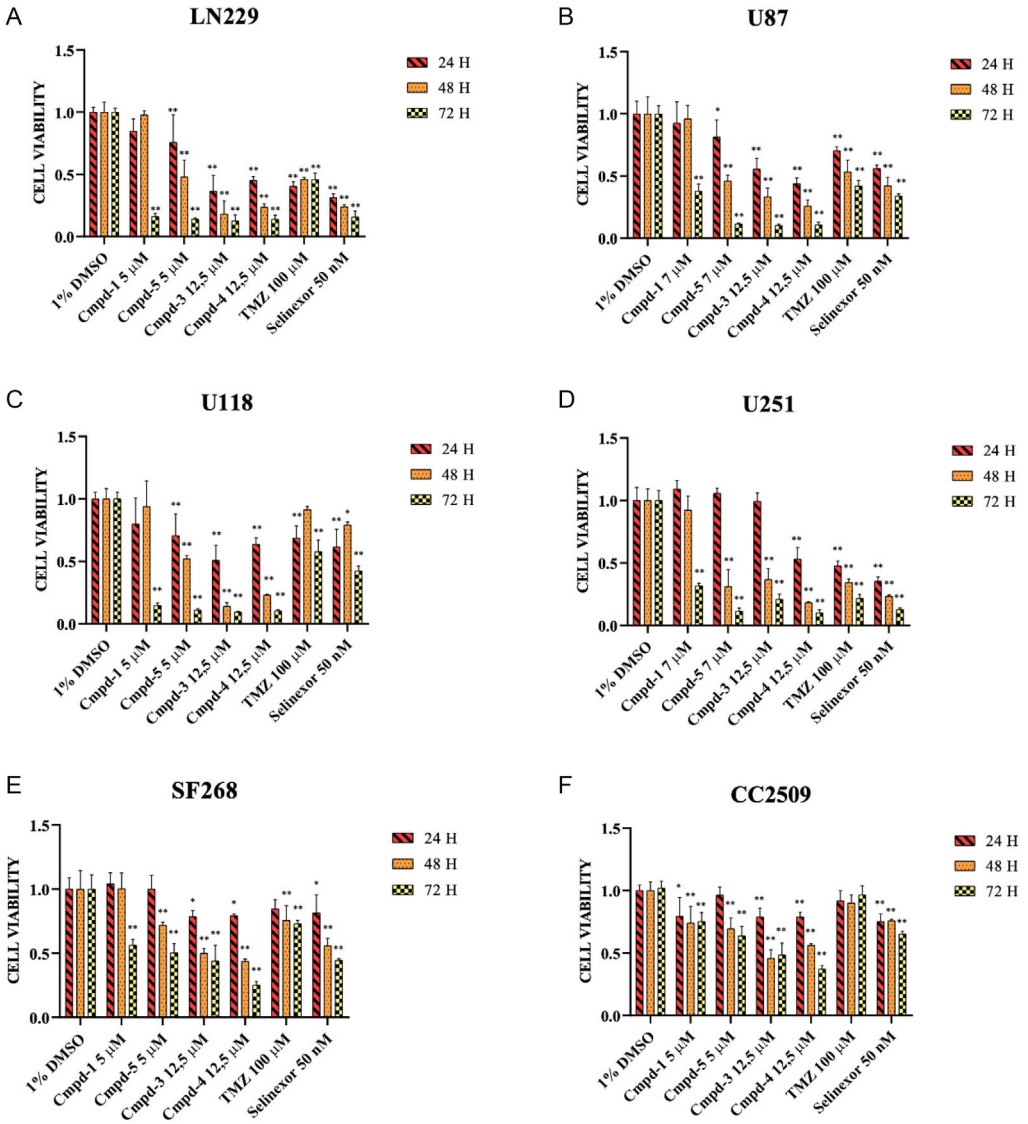

Figure 7. Cell viability in GB and CC2509 fibroblast cell lines is differentially affected following treatment with CRM1 inhibitors. GB and fibroblast cells were incubated for 24 h (red/stripes), 48 h (orange/dots), and 72 h (yellow/squares) with varying concentrations of compounds **1**, **5**, **3**, **4**, and selinexor. Names of the cells or cell lines in panels (A–F). Controls included 1% DMSO and 100 μM TMZ. Cell viability, normalized to DMSO controls, is shown on the Y-axis. Statistical significance is indicated as $*p < 0.05$, $**p < 0.01$, compared to the DMSO control.

involved in this aggressive cancer. In this study, we report the discovery of chromenone analogs that act as selective and potent inhibitors of CRM1-dependent nuclear export, demonstrating significant cytotoxicity against GBM cells. These findings underscore the potential of these compounds as effective therapeutic agents for targeting CRM1 in GBM treatment.

We utilized two reporter proteins, FOXO-GFP and NES-RFP, which rely on CRM1 for nuclear export through their NES sequences. These CRM1-dependent cargo proteins were ectopically expressed in an osteosarcoma cell line, and their coculture allowed the development of a previously established multiplexed assay system.[20] Using this multiplexed HCS assay system, we tested our hypothesis that chromenone compounds could inhibit the human CRM1 by binding to its cysteine residue at position 528.

Chromenones are an important class of oxygen-containing heterocyclic compounds with diverse biological activities and applications.[26] Importantly, Huo et al. showed that chromene derivatives can act as a probe to detect thiol-containing molecules.[23] A nucleophilic attack of thiols to the α,β-unsaturated ketone of the chromenone probe that resulted in a fluorescent signal has been postulated as a possible detection mechanism.[27] Indeed, we showed that the chromenone derivative **1** acts as a potent CRM1 inhibitor, as evidenced by its ability to induce nuclear retention of NES-tagged reporter proteins in a dose-dependent manner.

The CRM1 receptor facilitates the nuclear export of its substrates by binding to NESs within the cargo proteins. This interaction occurs within the NES-binding groove of CRM1, which positions the cargo in a conformation suitable for export through the nuclear pore complex.[28] The export process is regulated by RanGTP, a small GTPase, which stabilizes the CRM1-cargo complex and drives its translocation from the nucleus to the

cytoplasm. CRM1 is known to export a wide variety of substrates, including over 200 distinct proteins identified to date among them RANBP1 and COP1.[20] RANBP1 is a key regulatory protein that facilitates the dissociation of the CRM1-cargo complex after export by promoting RanGTP hydrolysis to RanGDP, thereby ensuring efficient recycling of the transport machinery. COP1 is an E3 ubiquitin ligase that targets specific proteins for ubiquitination and subsequent proteasomal degradation. The nuclear accumulation of these proteins in treated cells confirmed the effect of the chromenone analogs on endogenous CRM1 substrates. Importantly, the nuclear retention effect was observed within 30 min of treatment, indicating rapid CRM1 inhibition. The specificity of this activity was further supported by the inactivity of compound **2**, which lacks sufficient electrophilicity to engage in covalent interaction with Cys528, the key reactive residue in CRM1.

A detailed SAR analysis revealed key structural features that influence the efficacy of these inhibitors. Compounds with a five-membered carbonyl-containing ring, such as compounds **1** and **5**, were more potent than their six-membered counterparts, including **4**. However, this correlation between the lower steric hindrance and compound performance was offset in compound **4**, probably due to the presence of an electron-withdrawing nitro group. This suggests that the factors influencing the susceptibility to Cys528 attack may be convoluted, potentially involving a series of interdependent effects modulating the electrophilicity of the key double bond. Among the tested compounds, **5** demonstrated the highest activity, with an EC50 approximately four times lower than that of compound **1**. This result suggests that halogen substitution, such as the 7-bromo group in **5**, enhances CRM1-binding affinity or electrophilicity. Conversely, compound **7** showed initial activity but exhibited significant toxicity at higher concentrations, underscoring the need to balance potency and toxicity in drug design. Molecular docking studies further elucidated the binding dynamics of these chromenone derivatives. Active compounds aligned well within the NES-binding groove of CRM1, positioning their electrophilic double bonds for covalent interaction with Cys528. The lack of correlation between docking binding energies and biological activity suggests that covalent reactivity, rather than noncovalent binding affinity, is the critical determinant of CRM1 inhibition. Additionally, nitro-substituted compounds like **4** and **3** interacted with lysine residues in the NES-binding groove, stabilizing their binding poses and compensating for less favorable six-membered ring geometry.

The chromenone derivatives also demonstrated significant activity in GBM cell lines, inducing nuclear retention of FOXO3, a key endogenous CRM1 substrate. This activity was observed across multiple GBM cell lines (LN229, SF268, U87, U118, and U251), despite variations in baseline sensitivity. Notably, the compounds exhibited greater potency in GBM cells compared to nontumoral fibroblasts, highlighting their selective cytotoxicity and therapeutic potential. Cytotoxicity studies revealed time- and dose-dependent effects, with compounds **3** and **4** showing the highest potency, reducing cell viability to below 20% in most GBM cell lines within 24 h. While compound **5** required longer exposure to achieve comparable cytotoxicity, it demonstrated excellent potency after 72 h, with minimal toxicity to nontumoral fibroblasts. These findings underscore the potential of chromenone derivatives as CRM1 inhibitors with therapeutic applications for GBM. The observed SAR provides a framework for optimizing these compounds to enhance their efficacy and safety profiles. Future research should focus on validating these findings in vivo, exploring combination therapies with standard GBM treatments like TMZ or radiotherapy, and further elucidating the biochemical interactions underlying their activity. Collectively, these results suggest that chromenone derivatives, particularly **5** and **1**, represent promising candidates for the development of next-generation CRM1 inhibitors, offering hope for more effective GBM treatments.

4. Experimental Section

Chemical Synthesis

All reagents and solvents were reagent grade or were purified by standard methods before use. ^{1}H and ^{13}C NMR spectra were recorded on a Bruker 300 MHz spectrophotometer. Chemical shifts are reported in ppm (δ). The coupling constants, *J*, are reported in Hertz (Hz). All compounds were routinely checked by thin layer chromatography using precoated silica gel 60 F254, aluminum foil, and the spots were detected under UV light at 254 and 365 nm or were revealed spraying with 10% phosphomolybdic acid in ethanol.

General procedure

A solution of a suitable 2-hydroxybenzaldehyde (1 mmol) in THF (1.5 mL), 2-cyclopentenone or 2-cyclohexenone (2 mmol), and imidazole (1 mmol) was mixed with water. The mixture was stirred for 72 h at room temperature, and then it was diluted with water and extracted with ethyl acetate. The organic layer was dried over anhydrous Na_2SO_4 and concentrated under reduced pressure. The crude was purified by flash chromatography as described below.

7-phenyl-3,3a-dihydrocyclopenta[*b*]chromen-1(*2H*)-one (**1**): The title compound was prepared from 2-hydroxy-5-phenylbenzaldehyde and 2-cyclopenten-1-one. Purification by flash chromatography (CH_2Cl_2) and crystallization by diethyl ether gave compound **1** in 48% yield. ^{1}H NMR (400 MHz, $CDCl_3$) δ: 7.59–7.50 (3H, m); 7.50–7.41 (3H, m); 7.40–7.32 (1H, m); 7.31–7.29 (1H, m); 7.02 (1H, d, $J = 8.3$ Hz); 5.39–5.32 (1H, m); 2.81–2.71 (1H, m); 2.69–2.59 (1H, m); 2.47–2.31 (1H, m); 2.28–2.14 (1H, m). ^{13}C-NMR (100 MHz, $CDCl_3$) δ: 201.3; 154.8; 139.9; 135.6; 132.0; 131.1; 128.9 × 2C; 128.8; 127.7; 127.3; 126.7 × 2C; 122.2; 116.9; 76.0; 37.1; 28.1. HRMS (ESI) *m/z* calcd for $C_{18}H_{14}O_2Na$, $[M + Na]^+$: 285.0891, found: 285.0887.

7-phenyl-2,3,4,4a-tetrahydro-*1H*-xanthen-1-one (**2**): The title compound was prepared from 2-hydroxy-5-phenylbenzaldehyde and 2-cyclohexen-1-one. Purification by flash chromatography (CH_2Cl_2) and crystallization by diethyl ether gave compound **2** in 16% yield. ^{1}H NMR (400 MHz, $CDCl_3$) δ: 7.59–7.52 (4H, m); 7.48–7.40 (3H, m); 7.39–7.32 (1H, m); 6.98 (1H, d, $J = 8.4$ Hz); 5.11–5.02 (1H, m); 2.69–2.59 (1H, m); 2.59–2.50 (1H, m); 2.50–2.37 (1H, m); 2.22–1.99 (2H, m); 1.83–1.68 (1H, m). ^{13}C-NMR (100 MHz, $CDCl_3$) δ: 197.4; 15.4; 140.0; 135.4; 131.5; 130.7; 129.0 × 2C; 128.2; 127.2; 126.7 × 2C; 122.4; 116.4; 74.9; 38.9; 29.7; 18.1. HRMS (ESI) *m/z* calcd for $C_{19}H_{16}O_2Na$, $[M+Na]^+$: 299.1048, found: 299.1043.

7-nitro-3,3a-dihydrocyclopenta[*b*]chromen-1(*2H*)-one (**3**). The title compound was prepared from 5-nitro-2-hydroxybenzaldehyde and 2-cyclopenten-1-one. Purification by flash chromatography (CH_2Cl_2) and crystallization by diethyl ether gave the desired product **3** in 22% yield. The NMR spectra matched with those reported in the literature.[23]

7-nitro-2,3,4,4a-tetrahydro-1*H*-xanthen-1-one (**4**): The title compound was prepared from 5-nitro-2-hydroxybenzaldehyde and 2-cyclohexen-1-one. Purification by flash chromatography (ETP: ethyl acetate 4:1), gave compound **4** in 18% yield. The NMR spectra matched with those reported in the literature.[29]

7-bromo-3,3a-dihydrocyclopenta[*b*]chromen-1(*2H*)-one (**5**): The title compound was prepared from 5-bromo-2-hydroxybenzaldehyde and 2-cyclopenten-1-one. Purification by flash chromatography (CH_2Cl_2) and crystallization by diethyl ether gave compound **5** in 57% yield. The NMR spectra matched with those reported in the literature.[30]

7-bromo-2,3,4,4a-tetrahydro-*1H*-xanthen-1-one (**6**): The title compound was prepared from 5-bromo-2-hydroxybenzaldehyde and 2-cyclohexen-1-one. Purification by flash chromatography (CH_2Cl_2) and crystallization by diethyl ether gave the desired product in 25% yield. The NMR spectra matched with those reported in the literature.[31]

7-(4-bromophenyl)-3,3a-dihydrocyclopenta[*b*]chromen-1(*2H*)-one (**7**): The title compound was prepared from 4′-bromo-4-hydroxy-[1,1′-biphenyl]-3-carbaldehyde and 2-cyclopenten-1-one. Purification by flash chromatography (CH_2Cl_2) and crystallization by diethyl ether gave compound **7** in 70% yield. ^{1}H NMR (400 MHz, $CDCl_3$) δ: 7.60–7.53 (2H, m); 7.48 (1H, dd, $J = 2.4$ Hz, 8.3 Hz); 7.45–7.39 (3H, m); 7.27 (1H, d, $J = 2.4$ Hz); 7.01 (1H, d, $J = 8.3$ Hz); 5.39–5.30 (1H, m); 2.81–2.71 (1H, m); 2.70–2.59 (1H, m); 2.46–2.32 (1H, m); 2.28–2.14 (1H, m). ^{13}C-NMR (100 MHz, $CDCl_3$) δ: 201.2; 155.0; 138.8; 134.3; 132.2; 132.0 × 2C; 130.8; 128.6; 128.3 × 2C; 127.3; 122.3; 121.5; 117.0; 76.0; 37.1; 28.1. HRMS (ESI) *m/z* calcd for $C_{18}H_{13}O_2NaBr$, $[M + Na]^+$: 362.9997, found: 362.9998.

7-(4-bromophenyl)-2,3,4,4a-tetrahydro-*1H*-xanthen-1-one (**8**): The title compound was prepared from 4′-bromo-4-hydroxy-[1,1′-biphenyl]-3-carbaldehyde and 2-cyclohexen-1-one. Purification by flash chromatography (CH_2Cl_2) and crystallization by diethyl ether gave compound **8** in 60% yield. ^{1}H-NMR (400 MHz, $CDCl_3$) δ: 7.60–7.54 (2H, m); 7.49 (1H, d, $J = 2.1$ Hz); 7.46 (1H, dd, $J = 2.4$ Hz, 8.5 Hz); 7.44–7.38 (3H, m); 5.12–5.01 (1H, m); 2.69–2.59 (1H, m); 2.59–2.51 (1H, m); 2.50–2.37 (1H, m); 2.21–1.99 (2H, m); 1.83–1.67 (1H, m). ^{13}C-NMR (100 MHz, $CDCl_3$) δ: 197.4; 155.6; 139.0; 134.1; 131.9 × 2C; 131.2; 130.9; 130.5; 128.3 × 2C; 127.9; 122.5; 121.4; 116.5; 74.9; 38.8; 29.7; 18.0. HRMS (ESI) *m/z* calcd for $C_{19}H_{15}O_2NaBr$, $[M + Na]^+$: 377.0153, found: 377.0155.

Computational Methods: Ligand Structure Setup

All docked compounds (**1**, **2**, **3**, **4**, **5**, **6**, **7**, and **8**) had their structure optimized using quantum mechanics calculations. The Gaussian 09[32] software package was used, and B3LYP/6-31G* was chosen as the level of theory and the basis set.[33,34] All compound structures were centered at 0,0,0 (center of mass removal step) using the GROMACS editconf function.[35] The prepare_ligand4.py of AutoDock Tools 4[36] was used to convert the ligand to the required pdbqt format.

Computational Methods: Molecular Mechanics/MD Simulations

To develop a comprehensive ensemble docking protocol, we used MD simulations with GROMACS 2020.2,[37,38] employing the GROMOS 54A7[39,40] and the CHARMM36m[41,42] force fields. The simulations used the apo Homo Sapiens CRM1 structure (PDB id: 6TVO),[43] after removing the Mg^{2+} ion and the covalently bound Leptomycin B. All missing residues were reconstructed using the Modeller software[44] using the A chains of PDB structures 3NC1[45] and 3GKX[46] as templates. Six missing residues at the N-terminal (PAIMTM) were manually added in PyMOL.[47] The protonation states of titratable residues were defined using PypKa[48] with a dielectric constant (ε) of 15 and an ionic strength of 0.1 M. We parameterized a GTP molecule using the Automated Topology Builder 3.0[49] for GROMOS 54A7 and the CHARMM-GUI[50] for CHARMM 36 m and placed it in the GTP-binding site of the RanGTP to mimic the apo CRM1 form.[51] In the GROMOS simulations, the system was solvated with 37 195 SPC water molecules,[52] while in the CHARMM simulations, 37523 TIP3P water molecules[53,54] were used. All systems were neutralized with 5 Na^+ ions and underwent a two-step minimization procedure, using the steepest descent minimization algorithm with no constraints in the first, and the *p*-LINCS[55] and SETTLE[56] algorithms, for solute and water molecules, respectively, in the second. Each replicate was initialized for 100 ps in NVT with an integration step of 1 fs, followed by 50 ps in NPT with a 2 fs integration step. In the NVT ensemble, the v-rescale[57] thermostat maintained the temperature at 310 K with a coupling constant of 0.01 ps. In the NPT ensemble, the Parrinello–Rahman barostat[58] with a 2.0 ps coupling constant and an isothermal compressibility of 4.5×10^{-5} bar^{-1}. After system initialization, five replicates were run for each force field: 1 μs for GROMOS and 200 ns for CHARMM, both with a 2 fs integration step. The nonbonded interactions were updated every 20 steps and treated with a single cutoff of 1.4 nm and 1.2 nm for the GROMOS and CHARMM simulations, respectively. Beyond the cutoff, van der Waals interactions were truncated, and the Coulombic interactions were treated with the Particle-Mesh Ewald method.[59] The LINCS[60] and SETTLE[61] algorithms were used to constrain solute and water molecules, respectively.

Computational Methods: Ensemble Docking

Molecular docking calculations were performed using the GPU-accelerated version of AutoDock 4.[36,62] From the MD simulations, one structure every 1 ns was selected from each replicate across both force fields, resulting in 6000 structures. The residues of the NES-binding groove in the 6TVO structure (Table S1, Supporting Information) were defined, and all structures were aligned using the Cα of these residues with GROMACS trajconv function.[38] Docking boxes were created with a spacing of 0.375 Å, a size of (68, 94, 60), and centered at (−46.166, −21.972, −52.310). The autogrid4 tool[36] prepared the CRM1 structures for compound docking. All interactions between ligand and receptor were explored by the AutoDock Lamarckian Genetic Algorithm (LGA). A total of 1000 LGA runs (docking solutions) were performed for each ligand using standard AutoDock parameters except for the number of score evaluations per LGA run (35 000 000). Docking poses were filtered to retain only those where Cys528 could interact with the compounds, using a distance cutoff of 3 Å between the sulfur of Cys528 and the double bond C atoms in each compound that could be targeted by the cysteine nucleophilic attack.

Computational Methods: Cell Culture

We used U2OS WT and U2OS genetically modified (U2foxRELOC and U2redNES), as well as GBM cell lines LN229, U87, U251, U118, and SF268 and neonatal dermal human fibroblasts CC2509. Both U2foxRELOC and U2redNES were established previously.[20,63] These cell lines were sorted by FACS to ensure homogeneity of the population. All cell lines employed in this project were cultured in P100 Petri dishes (Falcon) in a medium constituted by Dulbecco's modified Eagle's medium supplemented with 10% of fetal bovine serum (Sigma–Aldrich), 100 IU mL^{-1} penicillin, 100 μg mL^{-1} streptomycin (Gibco) and 2 mM L-glutamine (Sigma–Aldrich). Cells were maintained in a humidified incubator at 37 °C and 5% CO_2 and passaged to new dishes when confluence was reached by using trypsin/EDTA (Cytiva). For the screening, dose–response and time-course assays, U2foxRELOC and U2redNES lines were cocultured at a density of 10^4 cells of each in each well in 200 μL of medium and incubated

for 24 h before starting compound treatment. Black 96-well plates with clear bottom (BD Biosciences) were used in these experiments.

Computational Methods: Multiplexed Reporter Assays

In order to identify CRM1 inhibitors, we added 2 μL of the different compounds (100×) diluted in DMSO to the medium of each well in the 96-well plates at concentrations of 50, 25, and 10 μM. As controls, we used 1% DMSO, a nontoxic concentration, 25 μM LY294002, and 100 nM selinexor. All treatments were tested in duplicates and incubated at 37 °C and 5% CO_2 for 1 h. Then, cells were fixed with 100 μL of 4% formaldehyde (Sigma–Aldrich) and 5 μg mL^{-1} of Hoechst 33342 (Sigma–Aldrich) for nuclei staining for 15 min in the dark and at room temperature. Finally, plates were washed with phosphate-buffered saline (PBS) 1X (IIB) and stored at 4 °C in 100 μL per well of PBS 1× and sodium azide 0.05% (Sigma–Aldrich).[21] Results were analyzed using DMIL LED FLUO inverted microscope (Leica) at a 20-fold magnification and photographs were taken with the camera Ds-2MBWc (Nikon) installed on the microscope and NIS-Elements F 3.0 software.

Computational Methods: Dose–Response Assays

To explore the effectivity range of the hit compounds, we performed a dose–response analysis. 24 h after seeding the cells in the 96-well plates, we replaced medium of each well with 100 μL of hit compounds diluted in new medium at different concentrations and in duplicates. Once treated, plates were fixated and stored as previously described for screening assays. Representative images of each condition were taken with Cell Observer Z1 microscope (Zeiss) at a 20-fold magnification, using the camera installed in the microscope and the ZEN 3.7 blue edition software (Zeiss) software. Nuclear retention of reporter proteins in each image was quantified using JaCoP plugin from FIJI software, which allowed us to distinguish nuclear localization measuring colocalization of Hoechst 33342 signal and the reporter proteins signal. The data from three biological replicates were processed with Microsoft Excel and GraphPad software in order to calculate the EC50 values and standard deviation using interpolation analysis.

Computational Methods: Time-Course Assays

24 h after seeding the 96-well plates with the reporter cell lines, wells were treated with hit compounds diluted in medium at concentrations based on their EC50. As positive controls, LY294002 and selinexor were used at 25 and 50 nM, respectively. DMSO was used at 1% as a negative control. We defined different positions in each well for the follow-up of the experiment. Throughout the experiment, live-cell imaging was carried out using Cell Observer Z1 microscope and ZEN 3.7 blue edition software. In time-course assays, to see the effect over time and compounds toxicity, compounds were present in culture medium throughout the entire experiment. In all experiments, we took images of every condition for 24 h. We performed these assays twice and in duplicates. During the whole experiment, plates were maintained at 37 °C and 5% CO_2. Images were taken with Cell Observer Z1 microscope at a 20-fold magnification. All this material and videos were edited and quantified using ImageJ/FIJI and ZEN 3.7 blue edition software.

Computational Methods: Immunofluorescence

Immunofluorescence assays were carried out to assess nuclear export inhibition of endogenous proteins. U2OS WT, LN229, U87, U251, U118, and SF268 cell lines were cultured independently in coverslips in 24-well plates (Falcon) at a 25.000 cells/well density. After 24 h of incubation in 1 mL of medium, each well was treated with the compounds of interest. We used 25 μM of compounds **3** and **4** and 10 μM of **1** and **5** for GB cell lines and 50 and 20 μM in U2OS cell lines. 1% DMSO and selinexor at 50 nM were used as controls. After 1 h of incubation, cells were fixed with formaldehyde 4% for 10 min and permeabilized with PBS with 1% of bovine serum albumin (BSA) (Sigma–Aldrich) and 0.1% Triton X-100 (Sigma–Aldrich) for 10 min. Subsequently, cells were incubated with blocking buffer (PBS 0,1% BSA) for 1 h at RT, after which coverslips were incubated overnight at 4 °C in a wet chamber with 20 μL of primary antibodies diluted in blocking buffer: FOXO3 (Cell Signaling, #2497), RANBP1 (Invitrogen, #PA1-080), COP1 (Abcam, #56 400). After 24 h, coverslips were washed three times with PBS previously to a 2 h incubation with 20 μL of solution of secondary IgG Alexa Fluor 488 (Invitrogen) diluted 1:200 in blocking buffer and 1:500 dilution of DAPI (Invitrogen). Finally, coverslips were washed three times with PBS and mounted with a drop of Prolong (Invitrogen). They were stored in the dark until processed with microscope Nikon Eclipse 90i and photographs were taken using DS-QiMc camera (Nikon) and NIS-Elements 3.01 software. Finally, images were edited with FIJI program.

Computational Methods: Cell Viability Assays

GBM cell lines and fibroblasts were seeded at a density of 5.000 and 3.000 cells per well, respectively, and incubated for 24 h in transparent 96-well plates (Falcon). To test toxicity levels of each treatment, cells were treated for 24, 48, and 72 h with the hit compounds, DMSO, 50nM selinexor, and 100 or 150 μM TMZ in triplicates. Compounds **1** and **5** were tested at 5 and 7 μM; **3** and **4** at 12.5 μM. After the 24, 48, and 72 h treatments, medium was removed and changed for 100 μL of MTT (Merck) dissolved in medium at a final concentration of 0.5 mg/mL. After a 4 h incubation at 37 °C, this medium was replaced with 100 μL of DMSO to dissolve formazan crystals and maintained for 30 min in agitation at room temperature. Finally, 570 nm absorbance was quantified using the spectrophotometer VersaMax Microplate Reader (Molecular Devices) and SoftMax Pro software. The absorbance values used resulted from subtracting background 630 nm absorbance from 570 nm absorbance. The results were compared to those of the mean value of DMSO control for each incubation time. ANOVA statistical analysis and plots were generated using GraphPad program.

Acknowledgements

This work was supported by a grant from Spanish Ministerio de Ciencia e Innovación/Agencia Estatal de Investigación and the European Regional Development Fund (PID2022-136654OB-I00 financed by MCIN/AEI /10.13039/501100011033/FEDER, UE). The authors acknowledge financial support from Fundação para a Ciência e a Tecnologia through grants 2022.10517.BD and CEECIND/02300/2017 (10.54499/CEECIND/02300/2017/CP1387/CT0031), and projects 2023.10710.CPCA.A2, UIDB/04046/2020 (10.54499/UIDB/04046/2020), and UIDP/04046/2020 (10.54499/UIDP/04046/2020). Mass spectrometry analyses were performed at the Mass Spectrometry facility of the Unitech COSPECT at the University of Milan (Italy).

Conflict of Interest

Wolfgang Link is the scientific co-founder of Refoxy Pharmaceuticals GmbH, Köln, Germany and is required by his institution to state so in his publications. The funders had no role in the design and writing of the manuscript.

Author Contributions

Salvatore Princiotto: methodology, software, investigation, writing—original draft, writing—review and editing, visualization. **Lucía Jiménez**: conceptualization, methodology, software, formal analysis, investigation, writing—review and editing, visualization, supervision. **Lucía Domínguez**: methodology, investigation, writing—review and editing. **João G. N. Sequeira**: methodology, software, formal analysis, writing—review and editing, visualization. **Cristiana Mourato**: methodology, formal analysis, investigation. **Alba Orea-Soufi**: investigation, supervision. **Bruno Santos**: investigation, supervision. **Sabrina Dallavalle**: conceptualization, validation, formal analysis, resources, data curation, writing—review and editing, visualization, supervision, funding acquisition. **Miguel Machuqueiro**: conceptualization, software, validation, resources, data curation, writing—original draft, writing—review and editing, visualization, supervision, funding acquisition. **Bibiana I. Ferreira**: conceptualization, validation, resources, writing—original draft, supervision, funding acquisition. **Wolfgang Link**: conceptualization, validation, resources, writing—original draft, writing—review and editing, visualization, supervision, project administration, funding acquisition. **Salvatore Princiotto** and **Lucía Jiménez** contributed equally to this work.

Data Availability Statement

The data that support the findings of this study are available in the Supporting Information of this article.

Keywords: chromenone · chromosome region maintenance 1/XPO1 · exportin 1 · glioblastoma · molecular docking · nuclear export inhibitors

[1] H. G. Wirsching, E. Galanis, M. Weller, *Handb. Clin. Neurol.* **2016**, *134*, 381.
[2] R. Stupp, W. P. Mason, M. J. van den Bent, M. Weller, B. Fisher, M. J. B. Taphoorn, K. Belanger, A. A. Brandes, C. Marosi, U. Bogdahn, J. Curschmann, R. C. Janzer, S. K. Ludwin, T. Gorlia, A. Allgeier, D. Lacombe, J. G. Cairncross, E. Eisenhauer, R. O. Mirimanoff, *N. Engl. J. Med.* **2005**, *352*, 987.
[3] R. McLendon, A. Friedman, D. Bigner, E. G. Van Meir, D. J. Brat, G. M. Mastrogianakis, J. J. Olson, T. Mikkelsen, N. Lehman, K. Aldape, W. K. A. Yung, O. Bogler, J. N. Weinstein, S. VandenBerg, M. Berger, M. Prados, D. Muzny, M. Morgan, S. Scherer, A. Sabo, L. Nazareth, L. Lewis, O. Hall, Y. Zhu, Y. Ren, O. Alvi, J. Yao, A. Hawes, S. Jhangiani, G. Fowler, et al., *Nature* **2008**, *455*, 1061.
[4] C. W. Brennan, R. G. W. Verhaak, A. McKenna, B. Campos, H. Noushmehr, S. R. Salama, S. Zheng, D. Chakravarty, J. Z. Sanborn, S. H. Berman, R. Beroukhim, B. Bernard, C. J. Wu, G. Genovese, I. Shmulevich, J. Barnholtz-Sloan, L. Zou, R. Vegesna, S. A. Shukla, G. Ciriello, W. K. A. Yung, W. Zhang, C. Sougnez, T. Mikkelsen, K. Aldape, D. D. Bigner, E. G. Van Meir, M. Prados, A. E. Sloan, K. L. Black, et al., *Cell* **2013**, *155*, 462.
[5] M. Colardo, M. Segatto, S. Di Bartolomeo, *Int. J. Mol. Sci.* **2021**, *22*, 4899.
[6] M. Fornerod, M. Ohno, M. Yoshida, I. W. Mattaj, *Cell* **1997**, *90*, 1051.
[7] A. Shen, Y. Wang, Y. Zhao, L. Zou, L. Sun, C. Cheng, *Neurosurgery* **2009**, *65*, 153.
[8] X. Liu, Y. Chong, Y. Tu, N. Liu, C. Yue, Z. Qi, H. H. H. Liu, Y. Yao, H. H. H. Liu, S. Gao, M. Niu, R. Yu, *J. Hematol. Oncol.* **2016**, *9*, 108.
[9] A. S. Azmi, M. H. Uddin, R. M. Mohammad, *Nat. Rev. Clin. Oncol.* **2020**, *18*, 152.
[10] H. Y. J. Fung, Y. M. Chook, *Semin. Cancer Biol.* **2014**, *27*, 52.
[11] F. Zanella, *Traffic* **2013**, *14*, 247.
[12] A. L. Green, S. H. Ramkissoon, D. McCauley, K. Jones, J. A. Perry, J. H. R. Hsu, L. A. Ramkissoon, C. L. Maire, B. Hubbell-Engler, D. S. Knoff, S. Shacham, K. L. Ligon, A. L. Kung, *Neuro. Oncol.* **2015**, *17*, 697.
[13] T. R. Reich, C. Schwarzenbach, J. B. Vilar, S. Unger, F. Mühlhäusler, T. Nikolova, A. Poplawski, H. I. Baymaz, P. Beli, M. Christmann, M. T. Tomicic, *Cell. Mol. Life Sci.* **2021**, *78*, 5587.
[14] B. I. Ferreira, B. Cautain, I. Grenho, W. Link, *Front. Pharmacol.* **2020**, *11*, 625.
[15] A. Chari, D. T. Vogl, M. Gavriatopoulou, A. K. Nooka, A. J. Yee, C. A. Huff, P. Moreau, D. Dingli, C. Cole, S. Lonial, M. Dimopoulos, A. K. Stewart, J. Richter, R. Vij, S. Tuchman, M. S. Raab, K. C. Weisel, M. Delforge, R. F. Cornell, D. Kaminetzky, J. E. Hoffman, L. J. Costa, T. L. Parker, M. Levy, M. Schreder, N. Meuleman, L. Frenzel, M. Mohty, S. Choquet, G. Schiller, et al., *N. Engl. J. Med.* **2019**, *381*, 727.
[16] L. Yuan, W. Lin, H. Chen, S. Zhu, L. He, *Angew. Chem., Int. Ed.* **2013**, *52*, 10018.
[17] J. Du, W. Ma, Q. Gu, Q. Yao, S. Long, W. Sun, J. Fan, X. Peng, *Sens. Actuators, B* **2019**, *287*, 118.
[18] Z. Li, M. Ren, L. Wang, L. Dai, W. Lin, *J. Mater. Chem. B* **2019**, *7*, 3431.
[19] Y. Lu, R. Jiang, B. Cui, M. Wang, J. Fang, F. Li, F. Kong, Y. Zhou, *Sens. Actuators, B* **2023**, *397*, 134662.
[20] L. Jimenez, V. Mayoral-Varo, C. Amenábar, J. Ortega, J. G. N. Sequeira, M. Machuqueiro, C. Mourato, R. Silvestri, A. Angeli, F. Carta, C. T. Supuran, D. Megías, B. I. Ferreira, W. Link, *Traffic* **2022**, *23*, 587, https://doi.org/10.1111/TRA.12872.
[21] C. Amenabar, L. Jimenez, C. Mourato, V. Mayoral-Varo, D. Megías, B. I. Ferreira, W. Link, *Methods Mol. Biol.* **2025**, *2871*, 163.
[22] E. H. Walker, M. E. Pacold, O. Perisic, L. Stephens, P. T. Hawkins, M. P. Wymann, R. L. Williams, *Mol. Cell* **2000**, *6*, 909.
[23] F. J. Huo, Y. Q. Sun, J. Su, J. Bin Chao, H. J. Zhi, C. X. Yin, *Org. Lett.* **2009**, *11*, 4918.
[24] Z. Liu, S. Chen, H. Wang, Y. Zhao, S. Dong, *Bioorg. Chem.* **2022**, *129*, 106221.
[25] L. Jimenez, L. Domínguez, C. Amenabar, G. Serrão, W. Link, B. I. Ferreira, B. Santos, *Methods Mol. Biol.* **2025**, *2871*, 171.
[26] M. Costa, T. A. Dias, A. Brito, F. Proença, *Eur. J. Med. Chem.* **2016**, *123*, 487.
[27] Y. Yang, F. Huo, C. Yin, A. Zheng, J. Chao, Y. Li, Z. Nie, R. Martínez-Máñez, D. Liu, *Biosens. Bioelectron.* **2013**, *47*, 300.
[28] B. Cautain, R. Hill, N. de Pedro, W. Link, *FEBS J.* **2015**, *282*, 445.
[29] M. T. Rodrigues, H. Santos, L. A. Zeoly, D. A. Simoni, A. Moyano, F. Coelho, *Arkivoc* **2020**, *2020*, https://doi.org/10.24820/ARK.5550190.P011.133.
[30] R. Nandhikumar, K. Subramani, *Orient. J. Chem.* **2018**, *34*, 2106.
[31] C. F. Nising, U. K. Schmid, M. Nieger, S. Bräse, *J. Org. Chem.* **2004**, *69*, 6830.
[32] "Gaussian 09 Citation | Gaussian.com," can be found under https://gaussian.com/g09citation/, n.d.
[33] H. M. Huffman, G. S. Parks, M. Barmore, *J. Am. Chem. Soc.* **1931**, *53*, 3876.
[34] S. H. Vosko, L. Wilk, M. Nusair, *Can. J. Phys.* **2011**, *58*, 1200.
[35] D. Van Der Spoel, E. Lindahl, B. Hess, G. Groenhof, A. E. Mark, H. J. C. Berendsen, *J. Comput. Chem.* **2005**, *26*, 1701.
[36] G. M. Morris, H. Ruth, W. Lindstrom, M. F. Sanner, R. K. Belew, D. S. Goodsell, A. J. Olson, *J. Comput. Chem.* **2009**, *30*, 2785.
[37] M. J. Abraham, T. Murtola, R. Schulz, S. Páll, J. C. Smith, B. Hess, E. Lindah, *SoftwareX* **2015**, *1–2*, 19.
[38] D. Van Der Spoel, E. Lindahl, B. Hess, G. Groenhof, A. E. Mark, H. J. C. Berendsen, *J. Comput. Chem.* **2005**, *26*, 1701.
[39] W. Huang, Z. Lin, W. F. Van Gunsteren, *J. Chem. Theory Comput.* **2011**, *7*, 1237.
[40] N. Schmid, A. P. Eichenberger, A. Choutko, S. Riniker, M. Winger, A. E. Mark, W. F. Van Gunsteren, *Eur. Biophys. J.* **2011**, *40*, 843.
[41] B. R. Brooks, R. E. Bruccoleri, B. D. Olafson, D. J. States, S. Swaminathan, M. Karplus, *J. Comput. Chem.* **1983**, *4*, 187.
[42] J. Huang, S. Rauscher, G. Nawrocki, T. Ran, M. Feig, B. L. De Groot, H. Grubmüller, A. D. MacKerell, *Nat. Methods* **2016**, *14*, 71.
[43] A. Shaikhqasem, A. Dickmanns, P. Neumann, R. Ficner, *J. Med. Chem.* **2020**, *63*, 7545.
[44] B. Webb, A. Sali, *Curr. Protoc. Bioinforma.* **2016**, *54*, 5.6.1.
[45] T. Güttler, T. Madl, P. Neumann, D. Deichsel, L. Corsini, T. Monecke, R. Ficner, M. Sattler, D. Görlich, *Nat. Struct. Mol. Biol.* **2010**, *17*, 1367.
[46] T. Monecke, T. Güttler, P. Neumann, A. Dickmanns, D. Görlich, R. Ficner, *Science* **2009**, *324*, 1087.
[47] "Support | pymol.org," can be found under https://pymol.org/support.html, n.d.
[48] P. B. P. S. Reis, D. Vila-Vicosa, W. Rocchia, M. Machuqueiro, *J. Chem. Inf. Model.* **2020**, *60*, 4442.
[49] A. K. Malde, L. Zuo, M. Breeze, M. Stroet, D. Poger, P. C. Nair, C. Oostenbrink, A. E. Mark, *J. Chem. Theory Comput.* **2011**, *7*, 4026.
[50] S. Jo, T. Kim, V. G. Iyer, W. Im, *J. Comput. Chem.* **2008**, *29*, 1859.

[51] T. Monecke, D. Haselbach, B. Voß, A. Russek, P. Neumann, E. Thomson, E. Hurt, U. Zachariae, H. Stark, H. Grubmuller, A. Dickmanns, R. Ficner, *Proc. Natl. Acad. Sci. U. S. A.* **2013**, *110*, 960–965.
[52] J. Hermans, H. J. C. Berendsen, W. F. Van Gunsteren, J. P. M. Postma, *Biopolymers* **1984**, *23*, 1513.
[53] W. L. Jorgensen, J. Chandrasekhar, J. D. Madura, R. W. Impey, M. L. Klein, *J. Chem. Phys.* **1983**, *79*, 926.
[54] E. Neria, S. Fischer, M. Karplus, *J. Chem. Phys.* **1996**, *105*, 1902.
[55] B. Hess, *J. Chem. Theory Comput.* **2008**, *4*, 116.
[56] S. Miyamoto, P. A. Kollman, *J. Comput. Chem.* **1992**, *13*, 952.
[57] G. Bussi, D. Donadio, M. Parrinello, *J. Chem. Phys.* **2007**, *126*, https://doi.org/10.1063/1.2408420/186581.
[58] M. Parrinello, A. Rahman, *J. Appl. Phys.* **1981**, *52*, 7182.
[59] T. Darden, D. York, L. Pedersen, *J. Chem. Phys.* **1993**, *98*, 10089.
[60] B. Hess, *J. Chem. Theory Comput.* **2008**, *4*, 116.
[61] S. Miyamoto, P. A. Kollman, *J. Comput. Chem.* **1992**, *13*, 952.
[62] D. Santos-Martins, L. Solis-Vasquez, A. F. Tillack, M. F. Sanner, A. Koch, S. Forli, *J. Chem. Theory Comput.* **2021**, *17*, 1060.
[63] F. Zanella, A. Rosado, F. Blanco, B. R. Henderson, A. Carnero, W. Link, *Assay Drug Dev Technol* **2007**, *5*, 333.

Manuscript received: March 4, 2025
Revised manuscript received: April 20, 2025
Version of record online: April 23, 2025